

Optimal Design of Electromagnetic Absorbers

R. Araneo and S. Celozzi

Department of Astronautic, Electrical and Energetic Engineering
University of Rome "La Sapienza", via Eudossiana 18, 00184 Rome, Italy
rodolfo.araneo@uniroma1.it, salvatore.celozzi@uniroma1.it

Abstract — A procedure for the optimal design of compact and light-weight electromagnetic absorbers is presented. The absorbers are designed to damp resonances inside metallic enclosures on the basis of Jaumann's theory; several layers of lossy (artificial) dielectrics are separated by two high/low impedance frequency selective surfaces and one resistive sheet. The constitutive parameters of the absorbing layers are optimized by means of the Particle Swarm Optimization method in order to maximize bandwidth and absorption rate of the structure in the GHz frequency range, where typically the first resonances of small enclosures occur.

Index Terms - Absorbing materials, electromagnetic shielding, finite integration technique, particle swarm optimization and shielding effectiveness.

I. INTRODUCTION

The design of layers capable of absorbing Electromagnetic (EM) waves has been afforded either in numerical studies, e.g., [1], [2] and in practical applications [3]. One of the most challenging benchmarks to test a design procedure for EM absorbers is represented by the resonances occurring in typical shielding enclosures. Metallic cabinets behave as overmoded cavities at working frequencies, and the twofold goal of avoiding unwanted emissions and improving immunity of shielded devices is accomplished by damping the EM field in the shielded region. The Shielding Effectiveness (SE) of an enclosure is usually quantified according to the IEEE Std. 299 in terms of the ratio of the incident over the shielded electric (magnetic) field at a selected point inside the enclosure; although, integral definitions have

been proposed and adopted [4], [5]. It is well known that resonances can dramatically deteriorate the screening performance of the enclosure, because the excited internal modes can enhance the field in the victim proximity and apertures may increase these effects. Resonances can be suppressed by lining the internal enclosure surfaces with properly designed absorbers.

Research into EM wave absorbers started in the 1930's, shortly after the advent of radar with the aim of developing materials capable to reduce the radar cross-section (radar absorbing materials) and camouflaging military devices (stealth technologies) [6]. Through the years, the interest in absorbing materials has spread to the commercial sector to reduce interferences resulting from a growing number of EM apparatus, reaching into the radio frequency band [7]. Nowadays, there is a rising demand for lighter weight and more highly absorbing materials in a number of applications [8]. Absorbers can be roughly classified into impedance matching and resonant absorbers, though many absorbers have features of both these classifications; traditional designs include pyramidal, tapered loading, matching layers and ferrite-based absorbers [9], as well as Salisbury [10], [11] and Dallenbach [12] screens, Jaumann absorbers [13], [14] and circuit analog absorbers based on the use of lossy frequency selective surfaces [14], [15].

In this work, a procedure for the design of absorbing materials for damping resonances inside shielded enclosures is presented. The aims of the study are to design and optimize the performances of an absorbing structure in the GHz range, where the first resonances of commercial enclosures occur and to maximize the bandwidth and minimize the reflection coefficient for oblique

angles of incidence. The layered structure is based on Jaumann's theory and on circuit analogy. The main idea of Jaumann's theory is based on the achievement of a cancelling interference between incident and reflected wave by means of adequate dimensions and properties of the multi-layer structure. Absorption is enhanced alternating dielectrics and inductive, capacitive or resistive sheets; four layers of lossy dielectrics, one loaded with lossy wires are considered and alternated with three lossy sheets, two of which are lossy capacitive/inductive frequency selective surfaces [16], [17].

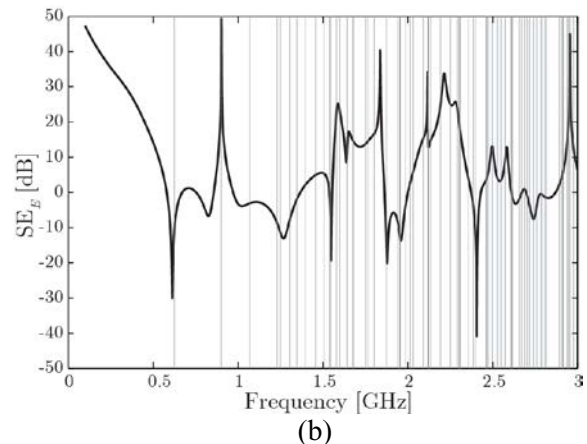
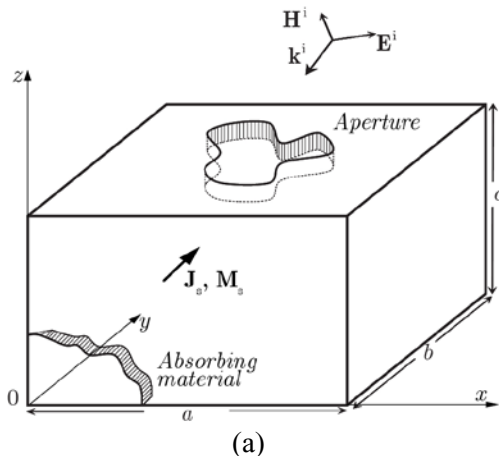
II. SYSTEM CONFIGURATION

The electromagnetic problem under analysis is sketched in Fig. 1 (a): a metallic enclosure, whose walls are assumed to be perfectly conducting and infinitesimally thin, presents an aperture on one side. When the enclosure is illuminated by an impinging external field \mathbf{E}^i or driven by internal sources, e.g., electric \mathbf{J}_s or magnetic \mathbf{M}_s dipoles [5], internal resonances can be excited deteriorating the shielding performances of the enclosure. As an example, in Fig. 1 (b), it is reported the electric field shielding effectiveness SE_E of a commercial enclosure, having dimensions $a \times b \times c = 30 \times 40 \times 12$ cm, with a rectangular aperture with dimensions $w \times h = 15 \times 3$ cm on its front side. Results are obtained by means of a Method of Moments (MoM) formulation [5] from 100 MHz to 3 GHz. The enclosure is illuminated with an y-directed uniform plane wave with the electric field linearly polarized along the shortest side of the aperture (i.e., the z-axis) and the

observation point is in the center of the enclosure ($E_z = 1$ V/m). In this frequency range, the enclosure exhibits 81 resonant frequencies as shown in Fig. 1 (b), with vertical grey lines (only the first 27 up to 2 GHz are reported in Table 1). It is evident that resonances and anti-resonances appear in the frequency spectrum of the SE_E , depending on the position of the observation point inside the cavity and on the resonant modes that are excited by the source field. Furthermore, Fig. 1 (c) shows the pattern of the first mode, while Fig. 1 (d) shows the maps of the magnitude of the electric field on the xy -plane and yz -plane passing for the center of the enclosure. As it is evident, the magnitude of the electric field at the first resonance is maximum at the center of the shielded box where the SE_E is evaluated, so that the shielding effectiveness presents there's a minimum.

In order to improve the SE_E , especially in the neighborhood of the resonant frequencies, the interior cabinet surfaces are lined with an artificial absorbing material to damp the excited resonant fields, as shown in Fig. 1 (a).

The design procedure proceeds in two steps: first, the layers characteristics are determined with reference to a set of plane wave sources having different incidence angles in the assigned frequency bandwidth. Then, the multilayer effectiveness is tested inside the enclosure in order to ascertain whether the initial goals have been met with the absorber in place. An iteration with more stringent constraints may be necessary or not, depending on the configuration and on the experience in fixing the initial target values.



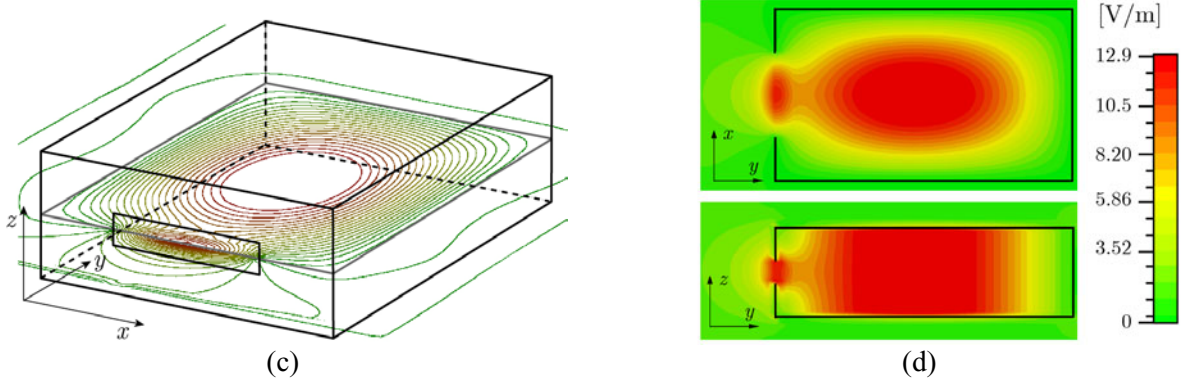


Fig. 1. (a) Shielded enclosure, with an aperture on one side, loaded with absorbing material in order to damp its resonances; (b) SE E versus frequency at the center of the shielded enclosure illuminated by an y-directed impinging plane wave: $a=30$ cm, $b=12$ cm, $c=40$ cm, rectangular aperture with dimensions $w=15$ cm, $h=3$ cm, centered in the xz -side; (c) electric field map at the first resonant frequency and (d) electric field patterns at the first resonant frequency in the center of xy -plane and yz -plane.

Table 1: Natural resonant frequencies up to 2 GHz of the 30×12 cm enclosure, along with the mode indices l , m and n

l	m	n	f [GHz]	l	m	n	f [GHz]
1	1	0	0.624	2	2	1	1.766
2	2	0	0.900	2	4	0	1.801
2	1	0	1.067	3	3	0	1.873
1	3	0	1.230	1	5	0	1.939
2	2	0	1.249	2	0	1	1.599
0	1	1	1.304	2	1	1	1.643
1	0	1	1.345	3	2	0	1.675
1	1	1	1.396	0	3	1	1.680
0	2	1	1.456	1	3	1	1.753
2	3	0	1.504	3	0	1	1.951
1	2	1	1.540	0	4	1	1.951
3	1	0	1.545	2	3	1	1.955
1	4	0	1.580	3	1	1	1.986

III. EQUIVALENT CIRCUIT REPRESENTATION

The proposed absorbing material consists of four dielectric layers alternated with three lossy sheets, as depicted in Fig. 2. The outer sheet is a capacitive array of patches, the middle sheet is a homogeneous resistive sheet and the inner sheet is an inductive strip-grid. Furthermore, the dielectric layer adjacent to the PEC surface is a wire-medium, realized by means of orthogonal wires in order to achieve a better polarization insensitivity.

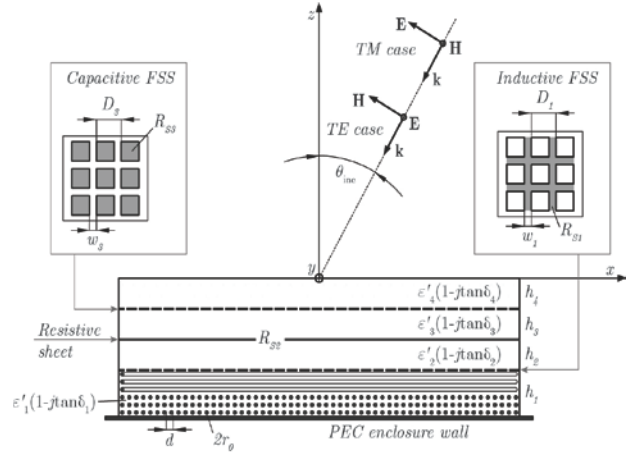


Fig. 2. Schematic of the multi-layer absorber; all the dielectrics are lossy $\epsilon_r = \epsilon'_r - j\epsilon''_r$ and the dielectric adjacent to the PEC surface is a wire-medium.

By proper selection of the geometrical and physical parameters of conductive sheets and dielectric layers, the result consisting in minimum EM field reflection over a prescribed frequency range and for oblique incidence angles is achieved. Particular effort has been devoted to make the absorber's characteristics as independent as possible of the incident angle [18]. To perform the design of the artificial material, an equivalent circuit representation is established by means of

equivalent surface impedances and quasi-dynamic formulas for effective parameters obtained through homogenization procedures [19]. The equivalent circuit representation is more suitable for the optimal tuning of the constitutive parameters.

The propagation of uniform plane-waves in homogeneous stratified media can be modeled by means of the analogy with voltage and current waves on uniform equivalent Transmission Lines (TLs) [20], [21]; any arbitrary incident plane wave is decomposed into its fundamental TE_z and TM_z polarized waves, as in Fig. 2. The propagation constants $k_{z,i}$ and the intrinsic characteristic impedance $Z_{c,i}$ of the i -th medium at angular frequency ω , are functions of both polarization and angle of incidence θ_{inc} as:

$$k_{z,i} = k_0 \sqrt{\epsilon_{r,i} - \sin^2 \theta_{inc}}, \quad (1a)$$

$$Z_{c,i}^{TE} = \frac{\omega \mu_0}{k_{z,i}}, \quad (1b)$$

$$Z_{c,i}^{TM} = \frac{k_{z,i}}{\omega \epsilon_0 \epsilon_{r,i}}, \quad (1c)$$

where $j = \sqrt{-1}$, k_0 is the wavenumber in free space, ϵ_0 and μ_0 are, respectively, the absolute permittivity and permeability of vacuum and $\epsilon_{r,i}$ is the relative electric permittivity of i -th medium. The square root branch in (1a) is specified by the condition $-\pi < \arg(k_{z,i}) \leq 0$. The free space surrounding the structure is modeled by a port with interior impedance Z_{fs} , according to (1b)-(1c), where $\epsilon_{r,i}$ is set equal to 1. Thus, the equivalent circuit reported in Fig. 3 is obtained.

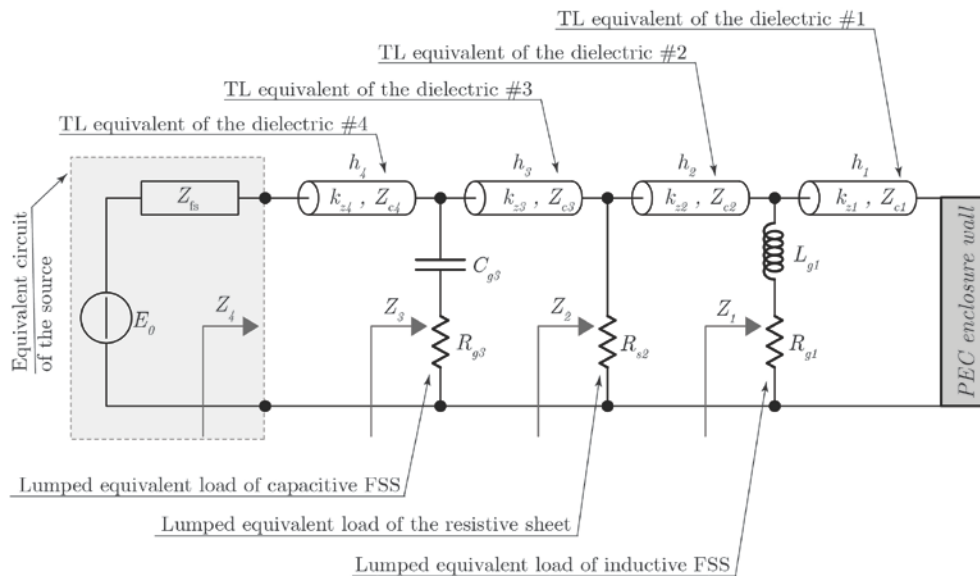


Fig. 3. Equivalent circuit model of the overall system; an equivalent EM field source (frequency-, polarization- and angle-of-incidence-dependent) incident on a multi-layer absorber.

To account for the three sheets located at the interfaces between dielectrics, equivalent lumped impedances are derived and inserted transversally in the equivalent circuit. An array of patches (outer interface #3), at frequencies well below the array resonances, exhibits an equivalent grid capacitance C_g [22]:

$$C_g^{TM} = \frac{2\alpha}{\eta_{eff} \omega}, \quad (2a)$$

$$C_g^{TE} = \frac{2\alpha}{\eta_{eff} \omega} \left(1 - \frac{\sin^2 \theta_{inc}}{2\mu_0 \epsilon_{eff}} \right), \quad (2b)$$

where α is the grid parameter:

$$\alpha = \frac{k_{eff} D}{\pi} \ln \left(\frac{1}{\sin \left(\frac{\pi W}{2D} \right)} \right), \quad (3)$$

and the effective (complex) permittivity is

function of the two adjacent dielectric permittivity's:

$$\epsilon_{\text{eff}} = \epsilon_0 \frac{\epsilon_{r,i} + \epsilon_{r,i+1}}{2}. \quad (4)$$

In (3), w is the width of the gap between adjacent patches, D is the period of the structure (as shown in Fig. 2), η_{eff} is the effective intrinsic wave impedance, $\eta_{\text{eff}} = \sqrt{\mu_0/\epsilon_0\epsilon_{\text{eff}}}$ and k_{eff} is the effective wavenumber, $k_{\text{eff}} = k_0\sqrt{\epsilon_{\text{eff}}}$. If the sheet is lossy, an equivalent resistance R_g should be inserted in series with the capacitance. According to [23], the resistance can be computed as:

$$R_g = \frac{R_s}{D-w} \frac{C_g}{\epsilon_{\text{eff}}}, \quad (5)$$

where R_s is the surface resistance of the sheet (measured in Ω/sq).

For a grid of strips (inner interface #1), the grid impedance is inductive. Through the Babinet's principle, the inductance can be derived straightforwardly from (2) as [22]:

$$L_g^{TM} = \frac{\eta_{\text{eff}}\alpha}{2\omega} \left(1 - \frac{\sin^2 \theta_{inc}}{2\mu_0\epsilon_{\text{eff}}} \right), \quad (6a)$$

$$L_g^{TE} = \frac{\eta_{\text{eff}}\alpha}{2\omega}, \quad (6b)$$

where (3)-(4) still hold, considering w as the strip width (see Fig. 2). If the sheet is lossy, an equivalent resistance R_g should be inserted in series with the inductance. According to [23], the resistance is:

$$R_g^{TE/TM} = \frac{R_s}{w} \frac{L_g^{TE/TM}}{\mu_{\text{eff}}}. \quad (7)$$

The homogeneous resistive sheet located at the interface #2, is represented by its surface resistance R_{s2} , as shown in Fig. 3.

The layers between sheets are assumed to be lossy dielectric with relative dielectric constant $\epsilon_{r,i} = \epsilon'_{r,i} - j\epsilon''_{r,i} = \epsilon'_{r,i}(1 - j\tan\delta_i)$, where $\tan\delta_i$ is the loss tangent of the i -th dielectric medium. The inner dielectric adherent to the PEC surface of the enclosure is an artificial lossy wire-medium, as shown in Fig. 2. In the long-wavelength limit, such a structure behaves like an homogeneous material whose effective relative permittivity is a frequency-dependent scalar quantity. In the case of E-polarized incident plane wave and lossy wires

with finite conductivity σ , the dielectric constant reads [24]:

$$\epsilon_{r,i} = \epsilon'_{r,i} - j\epsilon''_{r,i} = \epsilon_{r,h} + \frac{c_0\eta_0}{j\omega d^2(j\omega L + \zeta_s)}, \quad (8)$$

where c_0 is the free space speed of light, η_0 is the wave impedance in free space, d is the period of the wire grid and $\epsilon_{r,h}$ is the relative permittivity of the host medium. In (8), the per unit length external inductance of wires L is given by:

$$L = \frac{\mu_0\mu_{rh}}{2\pi} \ln \left[\frac{d^2}{4r_0(d-r_0)} \right], \quad (9)$$

being r_0 the wire radius. The per unit length impedance ζ_s , accounting for wire losses is:

$$\zeta_s = \frac{1+j}{2\pi r_0} \sqrt{\frac{\pi\eta_0 f}{c_0\sigma}} \frac{I_0(\xi)}{I_1(\xi)}. \quad (10)$$

In (10), $I_0(\cdot)$ and $I_1(\cdot)$ are, respectively, the modified Bessel functions of the first kind of order 0 and 1, and:

$$\xi = (1+j)\sqrt{\omega\mu_0\sigma} r_0. \quad (11)$$

In order to obtain a material effective under both TM_z and TE_z polarizations, two set of wires mutually perpendicular have been introduced in order to achieve polarization insensitivity.

The actual reflection coefficient Γ of the multilayered material at air/absorber interface #4, must be computed by using the well-known transmission line theory. Starting from the inner layer #1 and moving toward the free space, the input impedance Z_i at the beginning of the i -th line (assuming the line terminated at $l = h_i$ on the impedance Z_{i-1} , with $Z_0 = 0$ since the first line is terminated on the PEC surface of the enclosure) is evaluated:

$$Z_i = Z_{c,i} \frac{Z_{i-1} + Z_{c,i} \tanh(jk_{z,i}h_i)}{Z_{c,i} + Z_{i-1} \tanh(jk_{z,i}h_i)}. \quad (12)$$

Then the impedance value Z_i is updated by performing the parallel of the computed Z_i with the lumped sheet admittance Y_i^{sheet} (we assume $Y_4^{\text{sheet}} = 0$ since there is no sheet at the air/absorber interface), according to:

$$Z_i = \left(\frac{1}{Z_i} + Y_i^{\text{sheet}} \right)^{-1}. \quad (13)$$

Finally, once the Z_4 is available, the reflection coefficient (to be minimized) of the absorbing material can be computed as:

$$\Gamma = \frac{Z_4 - Z_{fs}}{Z_4 + Z_{fs}}. \quad (14)$$

It should be noted that Γ has to be minimized in a prescribed frequency range and for various incidence angles and polarizations.

IV. OPTIMIZATION

To optimize all the geometrical and constitutive parameters of the absorbing material in order to reduce its reflection coefficient Γ in the prescribed frequency range, the Particle Swarm Optimization (PSO) has been used. Several metaheuristic evolutionary algorithms are available today, such as the Genetic Algorithm (GA), the Ant Colony Optimization (ACO), the Bees Algorithms and the PSO, and they have been applied successfully in the design of absorbing materials [25]-[28]. Since its proposal by Kennedy and Eberhart in 1995 [29], the PSO has rapidly become very popular as an efficient optimization method for solving single objective and multi-objective optimization problems. In addition, a large number of works dealing with the application of the PSO technique to engineering problems, is available in literature [30]-[34] and the authors have developed a good expertise with this method in several past works [7], [34]-[36]. For these reasons, the PSO have been selected for the optimization process.

In the present work, a simple variation of the original PSO, referred to as Meta Particle Swarm Optimization (MPSO) [27] is adopted. It simply consists in subdividing the entire swarm in more subgroups of particles moving through the space domain \mathcal{D} . Each j -th group is composed of M_j particles flying with a velocity vector $\mathbf{v}_t^{m,j} = [v_{1,t}^{m,j}, v_{2,t}^{m,j}, \dots, v_{N,t}^{m,j}]^T$, at time t (with $m=1, 2, \dots, M_j$), around a multidimensional search space \mathcal{D} . During its flight, each particle updates its position $\mathbf{x}_t^{m,j} = [x_{1,t}^{m,j}, x_{2,t}^{m,j}, \dots, x_{N,t}^{m,j}]^T$ according to its own experience, to that of the group, which the particle belongs to and to the experience of the entire warm. The MPSO method combines three search levels:

1. A local single-particle search: the m -th particle knows its personal best position $\mathbf{b}_L^{m,j}$ (local optimum solution); i.e., the coordinates associated with the best solution that the particle has achieved so far.
2. A group local search: the m -th particle exchanges information with other particles of the same group and knows the \mathbf{b}_S^j value (global optimum solution inside the j -th group); i.e., the coordinates associated with the best position even tracked by the group giving the best fitness value in the group population.
3. A swarm global search: the m -th particle exchanges information with all other particles and knows the best global value \mathbf{b}_G (global optimum solution); i.e., the coordinates associated with the best position even tracked by the swarm giving the best fitness value in the entire population.

At each algorithm step, $\mathbf{b}_L^{m,j}$, \mathbf{b}_S^j and \mathbf{b}_G are computed, updated and used by the particles to adjust their velocities and positions in order to improve their current fitness through the following two updating equations:

$$\mathbf{v}_{t+1}^{m,j} = w\mathbf{v}_t^{m,j} + c_1\phi_1(\mathbf{b}_L^{m,j} - \mathbf{x}_t^{m,j}) + c_2\phi_2(\mathbf{b}_S^j - \mathbf{x}_t^{m,j}) + c_3\phi_3(\mathbf{b}_G - \mathbf{x}_t^{m,j}), \quad (15a)$$

$$\mathbf{x}_{t+1}^{m,j} = \mathbf{x}_t^{m,j} + \mathbf{v}_{t+1}^{m,j}. \quad (15b)$$

The entire optimization relies on the correct manipulation of the particles' velocities; w is the inertia factor, which keeps the particle in its current trajectory. The last three terms inject deviation according to the distances from $\mathbf{b}_L^{m,j}$, \mathbf{b}_S^j and \mathbf{b}_G best locations through the cognitive factor c_1 , the group social factor of the j -th group c_2 and the global social factor c_3 . The numbers ϕ_1 , ϕ_2 and ϕ_3 are random variables distributed in the range $[0,1]$, which inject the unpredictability of the particles' movement. The convergence of the algorithm depends on the proper tuning of the acceleration coefficients and on the boundary conditions used to prevent the explosion of the particles [37].

It should be noted that all the groups interact among them in the optimization process. In the

early time of the iteration process, the global best particle \mathbf{b}_G appears in every subgroup alternately, which shows the well global exploration performance that tends to concentrate in the territory around the group best particle \mathbf{b}_S^j in the medium time of the process. Then, when the algorithm enters the latter time of the process, \mathbf{b}_G is almost fixed in some subgroup and the algorithm begins with a local research around the best position tracked by the swarm. Several papers [38], [39] have introduced additional factors in the velocity equation; named repulsive factors in order to encourage individual particles, located in the territory of other groups to escape from the other groups' territory in efficient manners and consequently search for multiple optima in the solution space.

In the problem at hand, each particle $\mathbf{x}_{j,t}^{m,j}$ consists of a possible set of values for the constitutive/geometrical parameters of the absorbing material. The inertia and acceleration coefficients have been chosen according to [37] and the reflecting boundary conditions have been used to relocate the particles that fly outside the allowed solution space. The cost function \mathcal{F} that needs to be minimized is defined as:

$$\mathcal{F} = \frac{1}{2N_{freq}N_{inc}} \sum_{l=TE,TM} \sum_{m=1}^{N_{freq}} \sum_{n=1}^{N_{inc}} \left| \Gamma_l(\omega_m, \theta_{inc,n}) - \Gamma_0 \right|^2, \quad (16)$$

where N_{freq} is the number of sampling frequencies ω_m distributed over the band of interest, N_{inc} is the number of angles of incidence $\theta_{inc,n}$, Γ_0 is the target value to be achieved and $\Gamma_l(\omega_m, \theta_{inc,n})$ is the computed actual value of the reflection coefficient.

V. RESULTS

The methodology has been applied for the design of two absorbers in the frequency range from 100 MHz up to 3 GHz. The first one is constrained to possess best performance below 1 GHz because it is aimed at absorbing the first resonant modes. The second one is designed to absorb the higher modes of the enclosure occurring at frequencies above 1 GHz.

The following constraints have been enforced:

1. The periods D_1 and D_3 of both the selective surfaces (patch array and strip-grid) have been considered equal (through several simulations we have found that the optimum solution is near the condition $D_1=D_3$, so that this constrain has been directly enforced in the optimization process in order to obtain a simpler absorber).
2. The host dielectric of the wire-medium (medium #1) has been considered to be foam, $\epsilon_{rh} = 1$.
3. The loss tangent of all the remaining dielectrics has been set equal to 1.25×10^{-4} .
4. The two frequency selective surfaces have been considered lossless.

The geometrical variables and physical parameters that have been optimized are reported in Table 2 with their "optimum" values.

Table 2: Optimized values of the constitutive parameters of the absorber obtained through the PSO

Parameter	Absorber #1	Absorber #2
ϵ_2	9.9	4.5
ϵ_3	2.6	1.2
ϵ_4	5.9	2.9
h_1	4.8 mm	1.6 mm
h_2	5.5 mm	1.6 mm
h_3	5.8 mm	1.7 mm
h_4	6 mm	2 mm
$D_1=D_3$	22.8 mm	18.4 mm
w_1	0.8 mm	0.2 mm
w_3	2.2 mm	1.8 mm
R_{s2}	81.5 Ω /sq	243.7 Ω /sq
d	1 mm	0.3 mm
r_0	10 μm	5 μm

The frequency spectrum of the reflection coefficients Γ for both TM_z and TE_z polarizations are reported in Figs. 4, for different angles of incidence θ_{inc} for either of the absorbers. In all the Figs., it also reported the frequency trend of the prescribed reflectivity Γ_0 , that has been assumed equal to a band-pass Chebyshev filter of second type of order 4, for the design of the absorber #1 and 5, for the design of the absorber #2, with stop-band ripple equal to 10 dB and stop-band-edge

frequencies equal to 100 MHz and 3 GHz in either cases. The absorbing performance are not substantially degraded, increasing the incidence angle θ_{inc} . It is possible to note that under TM_z polarization, the absorbing performance of the two

absorbers are less stable with respect to the angle of incidence; nevertheless, they show higher absorbing coefficients for all the angles of incidence.

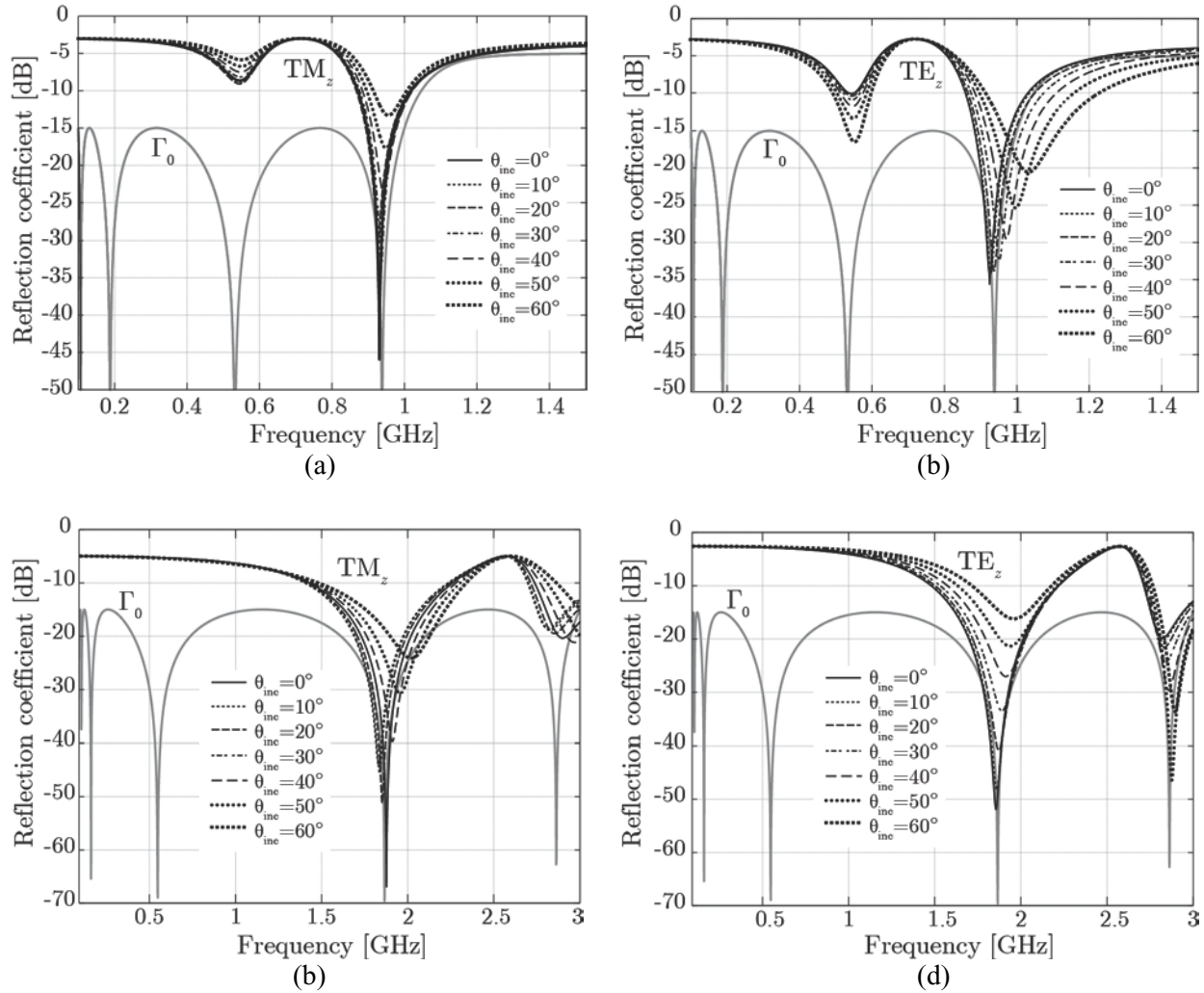


Fig. 4. Reflection coefficients Γ of the two absorbers versus frequency f for TM_z and TE_z polarizations for different angles of incidence θ_{inc} .

For the sake of completeness, the best value \mathbf{b}_G and the mean value of the swarm (that has been subdivided in 4 tribes) during the search are reported in Figs. 5, for both the absorbers. It is evident that after a very steep descent in the first steps, the tribes move slowly but quite constantly toward the best solution.

Finally, the shielding effectiveness SE_E of the commercial enclosure studied in Figs. 1, having dimensions $a \times b \times c = 30 \times 40 \times 12$ cm, with a

rectangular aperture with dimensions $w \times h = 15 \times 3$ cm on its front side, has been newly computed twice under a perpendicularly impinging plane wave ($\mathbf{E} = E\hat{z}$ and $\mathbf{k} = k\hat{y}$); a first time with absorber #1 placed on its interior walls, then with absorber #2. The results have been obtained by means of the Commercial Software CST Microwave Studio based on the Finite Integration Technique in the Time Domain. The results are reported in Figs. 6. It is possible to note that the

absorbers are effective in damping the effect of the first resonant frequencies of the shielded enclosure and their performance are reasonable compared to their geometrical dimensions and the values of their constitutive parameters. The attenuation shown by both the absorbers when placed inside the test enclosure are substantially in accordance with the theoretical predictions under plane wave incidence, with variable angle of incidence θ_{inc} .

Finally, Figs. 7 show the pattern of the electric field at the first resonant frequency of the enclosure $f = 0.624$ GHz, without (Fig. 7 (a)) and with (Fig. 7 (b)) the absorber #1 on the interior sides of the walls of the enclosure.

The absorber is effective in reducing the magnitude of the resonant field mode, especially in the central zone of the enclosure.

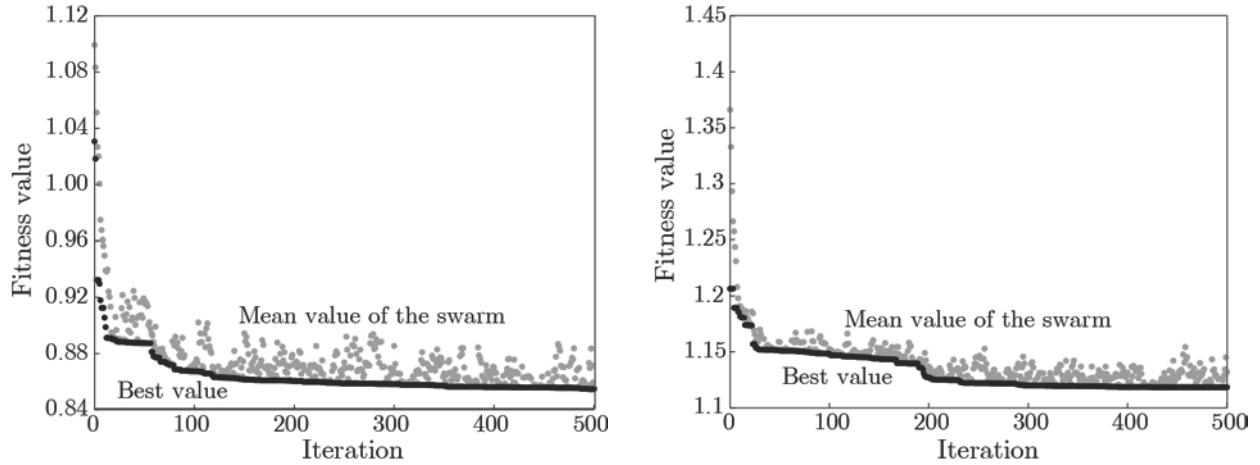


Fig. 5. Best value and mean value of the swarm during the optimization process.

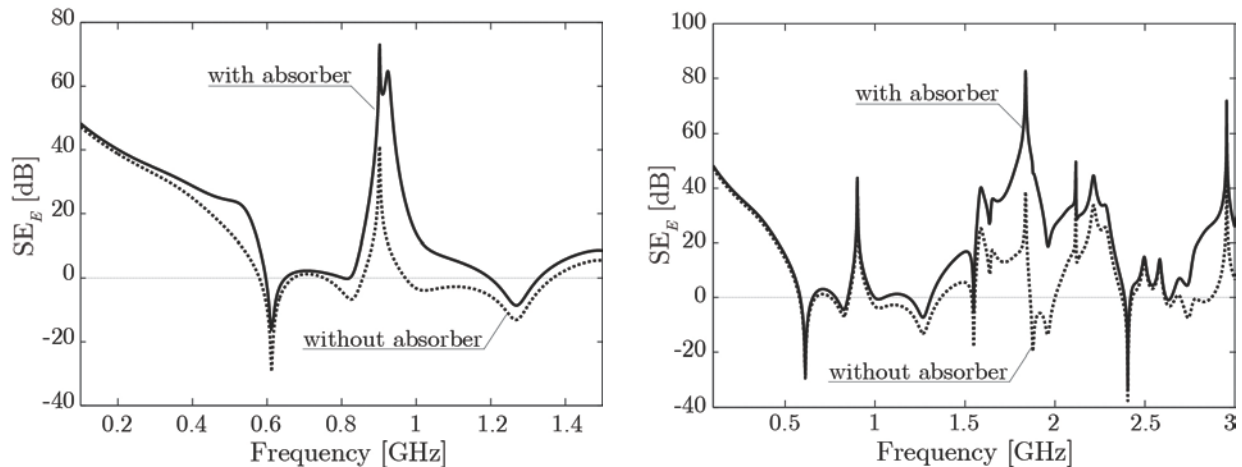


Fig. 6. Shielding effectiveness of the enclosure reported in Figs. 1, with and without the designed absorbers placed on its interior walls.

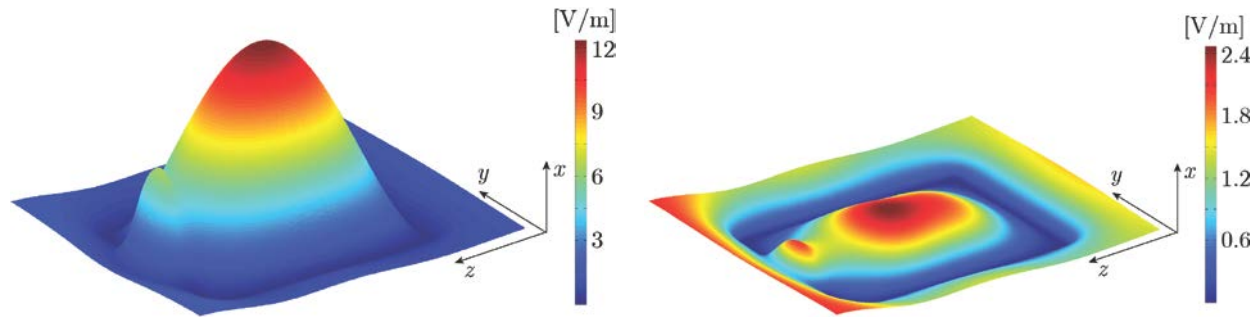


Fig. 7. Pattern of the electric field inside the enclosure at the first resonant frequency $f = 0.624$ GHz, with and without absorber #1.

VI. CONCLUSION

In this work, an optimal design procedure is presented, aimed at achieving compact and lightweight absorbing structures for damping resonances inside shielded enclosure. The proposed absorber is based on the concepts of Jaumann's layers and circuit analog absorbers; it employs four layers of lossy (artificial) dielectrics, separated by two high/low impedance frequency selective surfaces and one resistive sheet. The parameters of the absorber have been optimized by means of a PSO, in order to maximize its performance in the frequency range between 0.1 GHz and 3 GHz, for various incidence angles. The results show that an absorber with the expected performance can be obtained, demonstrating the effectiveness of the proposed design procedure and absorber configuration.

REFERENCES

- [1] W. Abdelli, X. Mininger, L. Pichon and H. Trabelsi, "Impact of composite materials on the shielding effectiveness of enclosures," *ACES Journal*, vol. 27, no. 4, pp. 369-375, 2012.
- [2] M. Agatonovic, Z. Marinkovic and V. Markovic, "Application of anns in evaluation of microwave pyramidal absorber performance," *ACES Journal*, vol. 27, no. 4, pp. 326-333, 2012.
- [3] E. A. Hashish, S. M. Eid and S. F. Mahmoud, "Design of wideband planar absorbers using composite materials," *ACES Journal*, vol. 24, no. 4, pp. 413-418, 2009.
- [4] S. Celozzi, "New figures of merit for the characterization of the performance of shielding enclosures," *IEEE Trans. Electromagn. Compat.*, vol. 46, no. 1, February 2004.
- [5] R. Araneo and G. Lovat, "Analysis of the shielding effectiveness of metallic enclosures excited by internal sources through an efficient method of moment approach," *ACES Journal*, vol. 25, no. 7, pp. 600-611, July 2010.
- [6] W. Emerson, "Electromagnetic wave absorbers and anechoic chambers through the years," *IEEE Trans. Antennas Propagat.*, vol. 4, pp. 484-490, July 1973.
- [7] R. Araneo, G. Lovat and S. Celozzi, "Shielding effectiveness evaluation and optimization of resonance damping in metallic enclosures," *In Proc. IEEE Asia-Pacific Electromagn. Compat. Symp.*, pp. 528-531, April 12-16, 2010.
- [8] E. Michielssen, S. R. J. M. Sajer and R. Mittra, "Design of lightweight, broad-band microwave absorbers using genetic algorithms," *IEEE Trans. Antennas Propagat.*, vol. 41, no. 6, pp. 1024-1031, June 1993.
- [9] F. L. Teixeira, "On aspects of the physical realizability of perfectly matched absorbers for electromagnetic waves," *Radio Science*, vol. 38, no. 2, VIC 15, pp.1-15, 2003.
- [10] W. W. Salisbury, "Absorbent body for electromagnetic waves," *US patent 2599944*, June 1952.
- [11] R. L. Fante, M. T. McCormack, T. D. Syst and M. A. Wilmington, "Reflection properties of the salisbury screen," *IEEE Trans. Antennas Propagat.*, vol. 36, no. 10, pp. 1443-1454, October 1988.
- [12] W. Dallenbach and W. Kleinsteuber, "Reflection and absorption of decimeter-waves by plane dielectric layers," *Hochfreq. u. Elektroak.*, vol. 51, pp. 152-156, 1938.
- [13] H. Severin, "Nonreflecting absorbers for microwave radiation," *In Electromag. Wave Theory Symp.*, vol. 7, pp. 385-392, 1956.
- [14] B. A. Munk, "Frequency selective surfaces: theory and design," New York: Wiley, 2000.
- [15] S. A. Tretyakov and S. I. Maslovski, "Thin absorbing structure for all incidence angles based on the use of a high-impedance surface," *Microw. Opt. Techn. Let.*, vol. 38, no. 3, pp. 175-178,

- August 2003.
- [16] R. Araneo, G. Lovat and S. Celozzi, "Shielding effectiveness of periodic screens against finite high-impedance near-field sources," *IEEE Trans. Electromagn. Compat.*, vol. 53, no. 3, pp. 706-716, August 2011.
- [17] G. Lovat, R. Araneo and S. Celozzi, "Dipole excitation of periodic metallic structures," *IEEE Trans. Antennas Propagat.*, vol. 59, no. 6, pp. 2178-2189, June 2011.
- [18] J. A. Gordon, L. Holloway and A. Dienstfrey, "A physical explanation of angle-independent reflection and transmission properties of metafilms/metasurfaces," *IEEE Antennas Wireless Propagat. Lett.*, vol. 8, pp. 1127-1130, 2009.
- [19] M. Silveirinha and C. Fernandes, "Homogenization of metamaterial surfaces and slabs: the crossed wire mesh canonical problem," *IEEE Transactions on Antennas and Propagation*, vol. 53, no. 1, pp. 59-69, January 2005.
- [20] K. A. Michalski and J. R. Mosig, "Multilayered media green's functions in integral equation formulations," *IEEE Trans. Antennas Propagat.*, vol. 45, no. 3, pp. 508-519, March 1997.
- [21] R. Araneo and S. Celozzi, "Analysis of the shielding performance of ferromagnetic screens," *IEEE Trans. Magn.*, vol. 39, no. 2, pp. 1046-1052, March 2003.
- [22] O. Luukkonen, C. Simovski, G. Granet, G. Goussetis, D. Lioubtchenko, A. V. Raisanen and S. A. Tretyakov, "Simple and accurate analytical model of planar grids and high-impedance surfaces comprising metal strips or patches," *IEEE Trans. Antennas Propagat.*, vol. 56, no. 6, pp. 1624-1632, June 2008.
- [23] F. Bilotti, A. Toscano, L. Vegni, K. Aydin, K. B. Alici and E. Ozbay, "Equivalent-circuit models for the design of metamaterials based on artificial magnetic inclusions," *IEEE Trans. Microwave Theory Tech.*, vol. 55, no. 12, pp. 2865-2873, 2007.
- [24] G. Lovat, P. Burghignoli and S. Celozzi, "Shielding properties of a wire-medium screen," *IEEE Trans. Electromagn. Compat.*, vol. 50, no. 1, pp. 80-88, February 2008.
- [25] J. B. Kim and J. H. Byun, "Salisbury screen absorbers of dielectric lossy sheets of carbon nanocomposite laminates," *IEEE Trans. Electromagn. Compat.*, vol. 54, no. 1, pp. 37-42, February 2012.
- [26] R. K. Gao, W. Hofer, T. S. Low and E. P. Li, "Robust design of electromagnetic wave absorber using the Taguchi method," *IEEE Trans. Electromagn. Compat.*, vol. 55, no. 6, pp. 1076-1083, December 2013.
- [27] S. Cui and D. S. Weile, "Application of a parallel particle swarm optimization scheme to the design of electromagnetic absorbers," *IEEE Trans. Antennas Propagat.*, vol. 53, no. 11, pp. 3616-3624, November 2005.
- [28] S. Genovesi, A. Monorchio, R. Mittra and G. Manara, "A sub-boundary approach for enhanced particle swarm optimization and its application to the design of artificial magnetic conductors," *IEEE Trans. Antennas Propagat.*, vol. 55, no. 3, pp. 766-770, March 2007.
- [29] J. Kennedy and R. C. Eberhart, "Particle swarm optimization," *In Proc. IEEE. Int. Neural Networks Conf.*, vol. IV, pp. 1942-1948, 1995.
- [30] A. Adly and S. K. Abd-El-Hafiz, "Utilizing particle swarm optimization in the field computation of non-linear magnetic media," *ACES Journal*, vol. 18, no. 3, pp. 202-209, 2003.
- [31] M. Farmahini-Farahani, R. Faraji-Dana and M. Shahabadi, "Fast and accurate cascaded particle swarm gradient optimization method for solving 2-d inverse scattering problems," *ACES Journal*, vol. 24, no. 5, pp. 511-517, 2009.
- [32] W. C. Weng, "Optimal design of an ultra-wideband antenna with the irregular shape on radiator using particle swarm optimization," *ACES Journal*, vol. 27, no. 5, pp. 427-434, 2012.
- [33] C. L. Li, C. H. Huang, C. C. Chiu and C. H. Sun, "Comparison of dynamic differential evolution and asynchronous particle swarm optimization for inverse scattering of a two-dimensional perfectly conducting cylinder," *ACES Journal*, vol. 27, no. 10, pp. 850-865, 2012.
- [34] R. Araneo, S. Celozzi and G. Lovat, "Design of impedance matching couplers for power line communications," *In Proc. IEEE Electromagn. Compat. Symp.*, pp. 64-69, August 17-21, 2009.
- [35] R. Araneo, S. Celozzi, G. Lovat and F. Maradei, "Multiport impedance matching technique for power line communications," *In IEEE Int. Symp. on Power Line Communications and Its Applications (ISPLC)*, pp. 96-101, 2011.
- [36] R. Araneo, S. Celozzi, G. Lovat and F. Maradei, "Computer-aided design of coupling units for naval-network power line communications," *In IEEE Int. Symp. on Industrial Electronics (ISIE)*, pp. 2961-2966, 2010.
- [37] M. Clerc and J. Kennedy, "The particle swarm: explosion, stability, and convergence in a multi-dimensional complex space," *IEEE Trans. Evol. Comput.*, vol. 6, pp. 58-73, February 2002.
- [38] J. H. Seo, C. H. Im, C. G. Heo, J. K. Kim, H. K. Jung and C. G. Lee, "Multimodal function optimization based on particle swarm optimization," *IEEE Trans. Magn.*, vol. 42, no. 4, pp. 1095-1098, April 2006.
- [39] D. K. Woo, J. H. Choi, M. Ali and H. K. Jung, "Anovel multimodal optimization algorithm

applied to electromagnetic optimization,” *IEEE Trans. Magn.*, vol. 47, no. 6, pp. 1667-1673, June 2011.



Rodolfo Araneo received his M.S. (cum laude) and Ph.D. degrees in Electrical Engineering from the University of Rome “La Sapienza”, Rome, in 1999 and 2002, respectively. Araneo received the Past President’s Memorial Award in 1999 from IEEE

Electromagnetic Compatibility (EMC) Society and won the best conference paper at the 2011 IEEE EMC Symposium. His research activity is mainly in the field of EMC and includes numerical and analytical techniques for modeling high-speed printed circuit boards, shielding and transmission line analysis. He has authored more than 110 papers in international journals and conference proceedings. He is coauthor of the book “Electromagnetic Shielding” published by John Wiley and Sons.



Salvatore Celozzi is Full Professor of Electrical Engineering with the Department of Astronautical, Electrical and Energetic Engineering at the University of Rome “La Sapienza”. Celozzi has published more than 120 papers in international journals or conference

proceedings, mainly in the fields of electromagnetic shielding and transmission lines. He served as Associate Editor of the IEEE Electromagnetic Compatibility (1995-2000) and authored a book on Electromagnetic Shielding for Wiley in 2008. His current research interests include transmission lines, electromagnetic compatibility, meta- and piezo-materials and numerical methods in electromagnetics.